A High-Efficient Power Converter for Thermoelectric Energy Harvesting

Van-Khoa Pham
Faculty of Electrical and Electronics Engineering
Ho Chi Minh City University of Technology and Education
Ho Chi Minh City, Vietnam
khoapv@hcmute.edu.vn

***Abstract*—Self-power technique is a vital key for stand-alone applications whereas battery replacement may be impossible. For wearable applications, extracting energy from the ambient temperature is one of the best solutions among the other energy harvesting methods such as solar, wireless waves, and temperature. In this paper, a high-efficient power dc-dc converter with maximum power point tracking (MPPT) and zero-current switching (ZCS) based on digital counters is proposed for thermoelectric energy harvesting. The proposed technique is able to adapt to a wide range of temperature differences. The integrated ZCS module plays an essential role in reducing the loss induced by inaccurately controlling the high-side switch. Besides, the maximum power extracted from the thermal energy source is monitored with the MPPT module. The power converter was simulated using CMOS 600nm Nuvoton technology. From the simulation results, it shows that when employing a thermoelectric generator with a temperature gradient of 3 Celsius degrees, the converter is capable of providing a maximum power of 112µW with a high-efficient of 66%.**

Keywords—thermoelectric generator (TEG), dc-dc booster, discontinuous conduction mode, zero-current switching (ZCS), maximum power point tracking (MPPT), counter-based controller

I. INTRODUCTION

Success in semiconductor and sensing technology has strongly supported the internet of things (IoT) concept in which a large number of devices can be wirelessly connected and communicated to each other. Wearable devices designed for specific applications have successfully applied the IoT concept. Ultra-low power consumption is a vital key in wearable applications because of the size constraints for batteries [1]. Even though circuit designs have been significantly optimized to consume as little power as possible [1]. However, battery capacity is determined by how long a wearable product can be operated properly [2]. For on-body applications, energy harvesting techniques from the ambient environments such as solar, wireless waves, and temperature

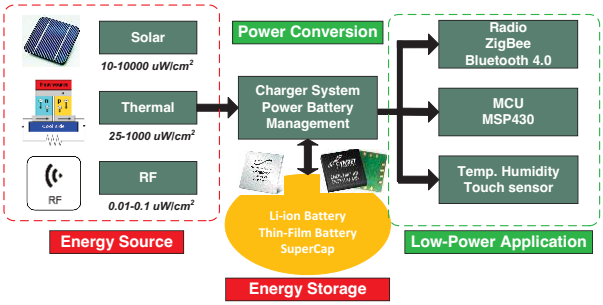

Fig. 1. Energy harvesting systems for wearable applications

have gained a lot of attraction from the circuit design community because the harvested power from renewable resources can substitute for conventional power delivery methods [3], [4], [5]. As demonstrated in Fig. 1, an energy harvesting system consists of three main parts: energy sources, power conversion, and energy storage devices. The power conversion plays an essential role in providing a high-efficiency output power for ultra-low-power applications [1-6].

In comparison to the other energy harvesting sources mentioned previously, thermoelectric generators (TEGs) seem to be suitable for wearable applications because the harvested power is only dependent on temperature conditions [6-9]. As depicted in Fig. 2a, a thermoelectric generator is constructed by a lot of thermocouple elements which are connected electrically in series. Based on the Seebeck effect [10], the output voltage from TEGs is proportional to the temperature gradient between the hot and cold sides. For the wearable applications, the hot and cold sides can be the surface of the skin and ambient environment, respectively [11]. It should be noted that the voltage level harvested from TEG devices is not high enough to power any digital circuitry. Therefore, a dc-dc converter is very essential to boost the low-voltage level generated by TEGs up to a useful voltage level for powering CMOS operations [1], [2].

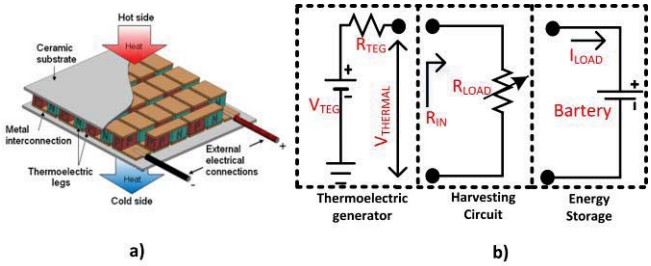

Fig. 2. a. Thermocouple structure [6] b. System overview of a thermoelectric energy harvesting system [3]

As shown in Fig. 2b, the system overview of a thermoelectric energy harvesting system consists of three parts: harvested source as TEGs, harvesting circuit, and energy storage. Where the magnitude of V_{TEG} reflects the temperature gradients applied on two sides of TEGs. The internal resistance (R_{TEG}) depends on the specific structure of TEG. For wearable applications, the TEG products from [12] introduce a large internal resistance as large as 185Ω. Here, the harvesting circuit is optimized to make the conversion ratio between the harvested power and the delivered power as high as possible.

$$Power\ eff.\ (\%) = \frac{P_{OUT}}{P_{IN}} \qquad (1)$$

From Equ. 1, it is obvious that we are able to obtain a high power efficiency when maximizing the delivery power

generated from the dc-dc converter. Based on the conversation law, the summation of the output power, the power consumption of the controller, switching, and synchronization losses as well is equivalent to the input extracted power from TEGs [4]. Therefore, power efficiency can be improved significantly if the power losses in the energy harvesting system are taken into account [1], [9]. To do so, switching signals need to be controlled properly to minimize synchronization losses. Also, it is very essential to utilize pure and simple digital circuits in implementing the dc-dc boost controller. This study aims to investigate the impacts of switching powers and synchronization losses. We proposed a high efficient power dc-dc boost converter in which the switching signals for both the low-side and high-side switches are controlled accurately to extract maximum input power from TEGs and minimize synchronization losses. By doing so, the digital controller is designed mainly for using counters which consume very low power.

II. Proposed Energy Harvesting Design

The proposed block diagram depicted in Fig. 3 consists of two main parts: the starter circuit and the main dc-dc boost converter. For on-body applications, the voltage output harvested from TEGs is extremely low and not sufficient for powering any CMOS circuitry. Therefore, the starter circuit is required in order to generate a higher voltage to start the main converter manually for the first time. This study aims to demonstrate the startup operation from 60mV. As shown in Fig. 3, the energy harvesting circuit is connected directly to the TEGs. After the starting process, the output voltage of the starter circuit, V_{DDS}, reaches 1.5. This voltage level is high enough to power the proposed digital MPPT-ZCS controller. The goal of the proposed design is to obtain a high voltage level as 4.2 V for charging energy storage devices such as big capacitors or batteries. In this way, wearable products can self-sustain its operation without external power sources.

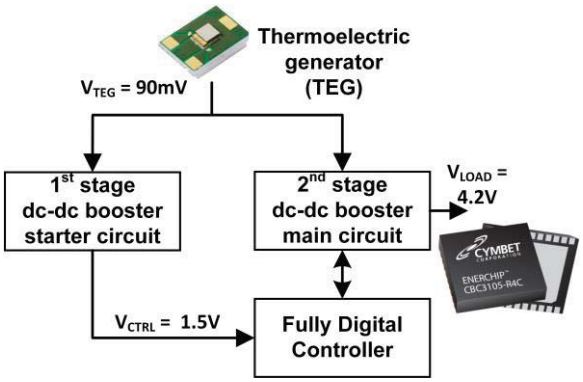

Fig. 3. The block diagram of the proposed thermoelectric energy harvesting system

According to the block diagram of the proposed thermoelectric energy harvesting system, the detailed schematic of the proposed system is demonstrated in Fig. 4. It includes two main parts: the starter circuit and main dc-dc boost converter in which the switching signals are controlled properly by the MPPT-ZSC controller. The input voltage node, V_{in}, for the converters is connected directly to single or array thermoelectric generators which are modeled by a voltage source V_{TEG} combined with a serial resistance R_{TEG}. Generally, the large capacitor, C_{in}, is needed in reducing the input-voltage ripple. Depicted on Fig. 4, for the starter circuit, the on/off switch, S1, linked with a serial resistor, R_{SW} is to illustrate a real mechanical switch that is activated by human. The switch will be pressed manually to start the main dc-dc boost converter. The diode, D, acted as the high side switch is made by a diode-connected transistor. The startup operation is explained as follows. If the switch S1 is pressed manually, the harvested current from TEGs will flow through the boost inductor L. After that, when the switch S1 is un-pressed, the energy stored on the inductor L will be released via the diode D in order to charge the output capacitor, C_{DDS}. By doing so, we can obtain the startup voltage as high as 1.5V when the energy flows into the capacitor C_{DDS}. This level voltage is helpful to power the operation of the main dc-dc booster. The high-efficient boost converter proposed in this study is based on conventional boost converters in which the high and low-side switches in discontinuous conduction mode are controlled properly. As shown in Fig. 4, the transistors, M_1 and M_2, are used to demonstrate the low-side and high-side switches, respectively. One thing that should be noted here is that the high-side switch, M_2, is essential for the boost converter to reduce significantly the power losses suffered by both the voltage drop and the synchronization, which will be explained in detail later.

The purpose of the MPPT-ZCS controller is to monitor the extracted power from TEGs and then adjust accurately the on-time for the switching signals on both the low-side and high-side switches using the digital switching signal QN and QP, respectively. The signal MPP is used to check periodically the average input voltage for the maximum power point tracking operation. Conceptually, we can obtain the maximum extracted power if the input voltage, V_{IN}, is maintained at half of V_{TEG}.

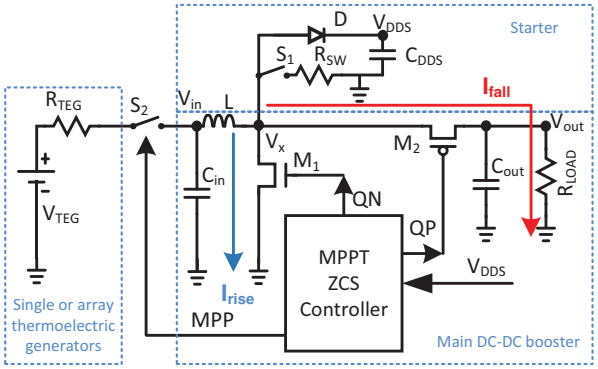

Fig. 4. The schematic of the proposed thermoelectric energy harvesting system

The waveforms in controlling both the low-side and high-side switches are presented in Fig. 5. As previously mentioned, the discontinuous conduction mode (DCM) applied to the boost converter for achieving a high-efficient conversion ratio is superior to the continuous conduction mode (CCM) [4]. By occupying DCM and an efficient control method for the main dc-dc boost converter, we can prevent the flowing negative current discharge the output capacitor C_{OUT} as depicted in Fig. 4. The previous studies [1], [2], [4] show that the negative current is the main reason to increase the synchronization power loss and switching loss as well. The waveforms in discontinuous-conduction mode shown by Fig. 5, in which T_1, and T_2 are the duty-adjustable

pulses for switching transistors M_1 and M_2, respectively. Besides, I_{RISE} and I_{FALL} are used to denote the current flows through the low-side and high-side switches, respectively. Based on the operation of the DCM, the magnitude of I_{RISE} is proportional to the on-time of the low-side switch.

Here, the switching frequency for boost converters should be considered carefully to optimize the conversion ratio. Equ. 2 shows the impact of the values for R_{TEG} and the induction L on the boost converter to the switching frequency [2].

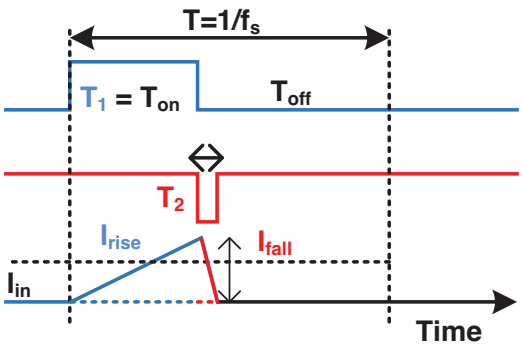

Fig. 5. The waveforms in discontinuous-conduction mode

$$f_s = \frac{R_{TEG}}{8L} \quad (2)$$

The prior study [9] claimed that a higher inductance can reduce the power losses significantly. Therefore, we used 100μH for the boost inductor L in this work because of the limitation of form-factor and a small equivalent series resistance as well. In addition, the thin-film thermoelectric generator used for our simulations [12] introduces a large internal resistance as 185Ω. If we use a duty cycle of 50 in controlling the low-side switch M_1. As a result, a very high-frequency in this case is required as calculated by Equ. 2. Even though the proposed converter is connected to an array of TEGs. If so, this results in an inefficient power converter. Because the experimental results [1] show that a high switching frequency of boost converters is not suitable in optimizing the switching power loss as well as power consumption. One more thing should be noted here, when using simple circuits, it is not easy to generate a high-frequency signal precisely to obtain an expected on-time level for the low-side switch M_1. Therefore, instead of changing the switching frequency, we realized a frequency as low as 20KHz combined with a duty-adjustable method for controlling the low-side switch M_1 in this work. Its operation will be explained later in this paper.

$$T_1 = \sqrt{\frac{2L}{R_{IN} * f_S}} \quad (3)$$

Once both the switching frequency, the boost inductor, and the internal resistance value of TEGs are given, the on-time, T_1, for the low-side switch M_1 should be controlled accurately as presented by Equ. 3 to implement the maximum power point tracking function.

III. Circuit Implementation

Fig. 6 shows conceptually the block diagram of the proposed fully digital controller including the MPPT and ZCS controller for the low-side and high-side switch, respectively. As mentioned above, to extract the maximum input power from TEGs, the dc-dc boost converter controls its internal impedance (R_{IN}) by adjusting the pulse width of T_1 to match R_{IN} with the R_{TEG}. To do so, a counter-based MPPT controller shown in Fig. 6a is proposed. It comprises two main parts: the voltage sensor and the duty controller. The voltage sensor is constructed by a low pass filter, voltage divider, and voltage comparator as well. The low pass filter is essential to have an average input voltage from TEGs. The input of the voltage divider is connected directly to the output of TEGs. The fact that the relationship between maximum power voltage point (V_{MPP}) and the open-circuit voltage (V_{TEG}) is almost linear [13]. Therefore, for thermoelectric energy harvesting applications, V_{MPP} should be calculated by the fractional open-circuit voltage as demonstrated in Equ. 4. By doing so, the counter-based MPPT controller will periodically isolate the thermoelectric generators with the boost converter and then measure the open-circuit voltage to determine the internal resistance of the converter is equivalent to the internal resistance or not. When the signal MPP is enabled, the outputs from both the low-pass filter and the voltage divider are applied to the voltage comparator. The comparison result is a binary level corresponding to the average input voltage level (V_{IN}) and half of V_{TEG}. If $V_{AVG} < V_{TEG}/2$, the comparator output is 0. On the contrary, the output signal will be 1 when $V_{AVG} > V_{TEG}/2$. After that, the comparison result synchronized by the MPPT_clk signal will determine whether or not the on-time pulse of the signal T_1 for the low-side switch should be increased.

$$P_{IN,MAX} = \frac{V_{TEG}}{2} * \frac{V_{TEG}}{2R_{TEG}} = \frac{V_{TEG}^2}{4R_{TEG}} \quad (4)$$

As mentioned previously, a 20Khz of frequency is utilized for switching the low-side switch M_1. According to the method proposed in [14], we used a tapped delay line in digital pulse width modulation (DPWM) block formed by a ring oscillator combined with a 4-bit up-down counter to adjust the pulse width of the switching frequency precisely. Delay elements formed by resistors and capacitors in the delay line are calculated carefully to have the accurate step size for adjusting the pulse width. By doing so, the DPWM in this study can adjust the pulse width with a resolution as small as 1.1μS to control the low-side switch M_1. As a result, the MPPT controller is able to cover a wide range of input voltage corresponding to a wide range of temperature changes. One thing should be noted here, the switch M_1 is made by a large-size power transistor. Therefore, the digital internal signal QN_D should be driven by a large-size buffer as shown in Fig. 6a.

To minimize the synchronization loss, the zero-current switching of the current stored on the L should be taken into account by controlling on-time for the high-side switch M_2 accurately. According to the conversation ratio between the input harvested voltage from TEGs (V_{IN}) and the boosted voltage (V_{OUT}) as shown in Fig. 4, the time for opening the switch M_2 can be calculated as the following equation

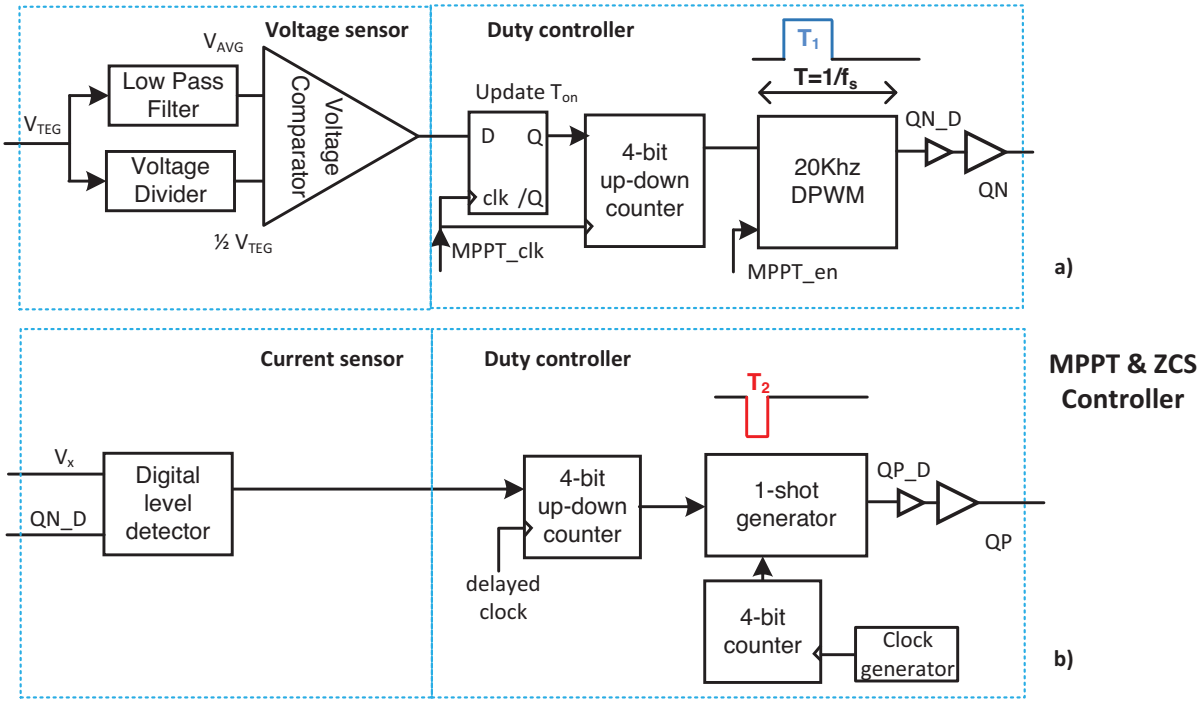

Fig. 6. The block diagram of the proposed fully digital controller a. counter-based MPPT controller and b. counter-based ZCS controller

$$\frac{T_2}{T_1} = \frac{V_{IN}}{V_{OUT}-V_{IN}} \quad (5)$$

As shown in Fig. 6b, a digital voltage level formed flip-flops is utilized to detect either the larger or a smaller voltage V_X in comparison to the output voltage level. According to the comparison result, if the high-side switch M_2 is controlled accurately, the latency allowing the inductor current to flow negative can be reduced. The input of the digital level detector includes the voltage level from the V_X node and the internal signal for controlling the low-side switch M_1. Based on the output of the flip-flop clocked by the QN_D signal, it will be defined as a high or low level. This signal is used to determine whether the 4-bit up/down counter in the proposed duty controller is increase or decrease values.

As described previously, for self-sustain wearable applications, we expect to obtain an output voltage as high as 4.2V for charging storage components like batteries. From Equ. 5, we can see that the conversation ratio in this study is as high as 35 if the harvested voltage of TEGs is 120mV at 2 Celsius degree temperature gradient. If the pulse width for opening the low-side switch M_1 is adjusted from 10μS to 25μS. As a result, the pulse width for the switch M_2 is varied from 300nS to 735nS. By using the 4-bit counter as shown in Fig. 6b, the pulse width resolution for the switch M_2 is around 27nS. From this analysis, the frequency for the clock generator depicted in Fig. 6b is defined to drive the 4-bit counter. The 1-shot generator constructed by a digital comparator will generate a pulse width QP_D for opening the switch M_2 properly based on the input counter values. In the same way with the signal QN_D, a driver is needed for the signal QP_D to drive a significant load as shown in Fig. 6b.

IV. Simulation Results

The operation of the proposed converter was verified using CMOS 600nm Nuvoton technology [15] and the Spectre Circuit Simulator [16]. Table I illustrates the design parameters of the converter. The voltage level for controlling the main dc-dc booster obtained from the startup process is defined as 1.5V. The internal resistance of TEGs is equivalent to 61Ω when three TEG devices fabricated by Mircopelt [12] are linked in parallel. As mentioned previously, the specification of the TEG [12] was modeled by a voltage source connected in series with an internal resistor using Verilog-A language [17] as shown in Fig. 4. For the boost circuit, the inductor value in this work is as high as 100μH to minimize the conduction loss and maintain the startup process. For the wearable applications such as a thermal harvester on the human body presented in [11], [13], it is not easy to make a large temperature gradient between the ambient environment and the body heat due to imperfect issues involving the mechanical design. Therefore, in this work, we evaluated the operation of the proposed boost converter when the input voltage from TEGs is changed from 60mV to 300mV. The limit of the voltage range corresponds to the 1 to 5 Celsius degree of the temperature difference applied to the TEGs. The output voltage of the dc-dc boost converter is expected as high as 4.2V for normal operation.

TABLE I. Design Parameters for the Energy Harvesting Circuit

Specification	Value
CMOS Technology	Nuvoton 600nm [15]
Seebeck voltage	60mV/°C [12]
Boost inductor	100μH
Impedance matching	61Ω
Control voltage	1.5V
Input voltage range	60 - 300mV
Output voltage	4.2V

The Fig. 7 shows the simulated results for the proposed thermoelectric energy harvesting system with the different applied temperatures on TEGs. The graph demonstrates the relationship between the power efficiency, the delivered power, and the applied temperatures. In this works, we assumed that the maximum temperature difference is as high as 5 Celsius degrees corresponding to 300mV of the harvested input voltage. As we can see that the proposed converter is able to obtain a high percentage of power efficiency as 64% when the input voltage is as low as 90mV. By performing the same simulation conditions with 3 Celsius degrees of the applied temperature, the converter can generate 112μW of the output power corresponding to 66% of the power efficiency. When the harvested input voltage is as low as 60mV with only 1 Celsius degree difference, the proposed converter is still operating. However, if the input voltage is lower than 60mV, the harvesting circuit will be halted because of low V_{DDS}. In this case, the converter requires a manual process to start the system again.

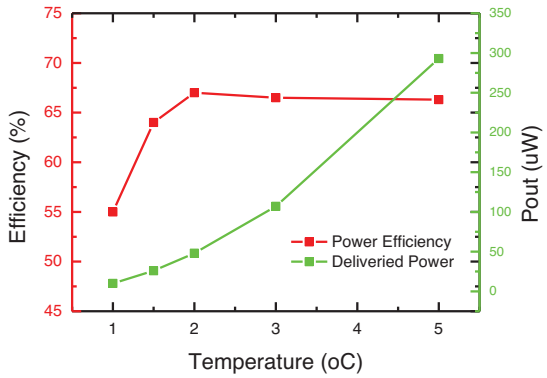

Fig. 7. power efficiency of the proposed thermoelectric energy harvesting system with the different applied temperatures

In addition, to demonstrate the impact of the operation of the maximum power point tracking module, we did a performance comparison between the harvesting circuit using MPPT and without the MPPT function. To do so, we use an enable signal MPPT_en from an external switch to define whether the converter is without or with the MPPT operation. As shown by Table II, it is obvious that the harvesting circuit combined with the proposed MPPT controller is able to tune the pulse width below 1μS in controlling the low-side switch M_1. The proposed circuit having the MPPT mechanism can achieve a higher power efficiency compared with non-MPPT at 180mV of the input voltage. The power efficiency difference is as large as 23% when the low-side switch M_1 is controlled by an inaccurate pulse width signal.

TABLE II. POWER EFFICIENCY COMPARISON USING THE MPPT APPROACH

Specification (V_{TEG}=180mV)	**T_1** **(μS)**	**Power Efficiency** **(%)**
MPPT	15.4	66
non-MPPT	13	43

V. CONCLUSION

In this study, we proposed a high-efficient power converter for wearable thermoelectric energy harvesting applications. A fully digital controller was designed to consider carefully power losses suffered by the un-matching internal resistance of the power converter when half of the harvested voltage from TEGs is not maintained as the input voltage as well as discharging the output capacitor when the high-side switch is not controlled accurately. The idea was verified using CMOS 600nm Nuvoton technology. From the simulation results, the proposed dc-dc boost converter can deal with a wide range of temperature changes. The power efficiency is maintained as high as 64% even though the harvested input voltage is as low as 90mV.

ACKNOWLEDGMENT

This work belongs to the project in 2020 funded by Ho Chi Minh City University of Technology and Education, Vietnam.

REFERENCES

[1] S. Bandyopadhyay, P. P. Mercier, A. C. Lysaght, K. M. Stankovic, and A. P. Chandrakasan, "A 1.1 nW Energy-Harvesting System with 544 pW Quiescent Power for Next-Generation Implants," *IEEE Journal of Solid-State Circuits*, vol. 49, pp. 2812 - 2824, 2014.

[2] Y. K. Ramadass and A. P. Chandrakasan, "A Battery-Less Thermoelectric Energy Harvesting Interface Circuit With 35 mV Startup Voltage," *IEEE Journal of Solid-State Circuits*, vol. 46, pp. 333 - 341, 2010.

[3] S. Bandyopadhyay and A. P. Chandrakasan, "Platform Architecture for Solar, Thermal, and Vibration Energy Combining With MPPT and Single Inductor," *IEEE Journal of Solid-State Circuits*, vol. 47, pp. 2199 - 2215, 2012.

[4] E. J. Carlson, K. Strunz, and B. P. Otis, "A 20 mV Input Boost ConverterWith Efficient Digital Control for Thermoelectric Energy Harvesting," *IEEE Journal of Solid-State Circuits*, vol. 45, pp. 741 - 750, 2010.

[5] Khoa Van Pham, etc., "A Thermoelectric Energy Harvesting Circuit For a Wearable Application," *Institute of Korean Electrical and Electronics Engineers*, vol. 21, iss. 1, pp. 66-69, 2017.

[6] S.B. Riffat and X. Ma, "Thermoelectrics: a review of present and potential applications," Applied Thermal Engineering, vol. 23, no. 8, pp. 913-935, Jun. 2003.

[7] M. Thielena, L. Sigristb, M. Magno, C. Hierolda, and L. Benini, "Human body heat for powering wearable devices: From thermal energy to application," *Science Direct*, vol. 131, pp. 44–54, 2017.

[8] J. Kim and C. Kim, "A DC–DC Boost Converter With Variation-Tolerant MPPT Technique and Efficient ZCS Circuit for Thermoelectric Energy Harvesting Applications," *IEEE Transactions on Power Electronics*, vol. 28, pp. 3827-3833, 2013.

[9] J. Katic, S. Rodriguez, and A. Rusu, "A Dual-Output Thermoelectric Energy Harvesting Interface With 86.6% Peak Efficiency at 30 µW and Total Control Power of 160 nW," *IEEE Journal of Solid-State Circuits*, vol. 51, pp. 1928 - 1937, 2016.

[10] S. Dalola, M. Ferrari, V. Ferrari, and M. Guizzetti, "Characterization of Thermoelectric Modules for Powering Autonomous Sensors," IEEE Transactions on Instrumentation and Measurement 2008.

[11] A. Myers, R. Hodges, and J. S. Jur, "Human and environmental analysis of wearable thermal energy harvesting," *Energy Conversion and Management*, vol. 143, pp. 218–226, 2017.

[12] TGP-651 Thin Film Thermogenerator, http://www.micropelt.com/fileadmin/user_upload/_PDF_TGP_UK.pdf.

[13] A. Paraskevas and E. Koutroulis, "A simple maximum power point tracker for thermoelectric generators," *Elsevier Energy Conversion and Management*, vol. 108, pp. 355-365, 2015.

[14] A. Syed, E. Ahmed, D. Maksimovic, and E. Alarcon, "Digital pulse width modulator architectures," *Power Electronics Specialists Conference*, 2004.

[15] https://www.nuvoton.com/

[16] https://www.cadence.com/en_US/home/tools/custom-ic-analog-rf-design/circuit-simulation/spectre-simulation-platform.html

[17] https://literature.cdn.keysight.com/litweb/pdf/ads2004a/pdf/verilogaref.pdf